Fibers and Polymers 2014, Vol.15, No.11, 2290-2296 DOI 10.1007/s12221-014-2290-5

Electrospinning and Microwave Absorption of Polyaniline/Polyacrylonitrile/ Multiwalled Carbon Nanotubes Nanocomposite Fibers

Zhichun Zhang, Fenghua Zhang, Xueyong Jiang, Yanju Liu[1], Zhanhu Guo[2], and Jinsong Leng*

Center for Composite Materials and Structures, Harbin Institute of Technology, Harbin 150080, P.R. China
[1]Department of Astronautical Science and Mechanics, Harbin Institute of Technology, Harbin 150001, P.R. China
[2]Integrated Composites Laboratory, Dan F. Smith Department of Chemical Engineering, Lamar University, Beaumont, TX 77710, USA

(Received March 18, 2014; Revised June 16, 2014; Accepted June 25, 2014)

Abstract: Electrical conductive nanocomposite fibers were prepared with polyaniline (PANI), polyacrylonitrile (PAN) and multi-walled carbon nanotubes (MWCNTs) via electrospinning. The morphology and electrical conductivity of the PANI/ PAN/MWCNTs nanocomposite fibers were characterized by scanning electron microscope (SEM) and Van De Pauw method. Electrical conductivity of nanocomposite fibers increased from 1.79 $S \cdot m^{-1}$ to 7.97 $S \cdot m^{-1}$ with increasing the MWCNTs content from 3.0 wt% to 7.0 wt%. Compared with PANI/PAN membranes, the mechanical property of PANI/PAN/MWCNTs nanocomposites fiber membranes decreased. The microwave absorption performance of composite films was analyzed using waveguide tube, which indicated that with the thickness increasing the value of R_L reduced from -4.6 to -5.9 dB.

Keywords: Fibers, Nano-structures, Polymer-matrix composites, Electrical properties

Introduction

Electrospinning, a kind of the effective methods to process polymers into continuous fibers with diameters ranging from micrometers to nanometers, has attracted significant interests in a host of fields [1,2]. Due to their large specific surface area, strong and mutual penetration, fine fabric structure, high aspect ratio, and better adsorption as well as filtration properties [3,4], nanofibers have been used in an array of fields such as biomedical functional materials [5-7], sensors [8], drug delivery [9], artificial blood vessels [10], fuel cell membranes [11], super hydrophobicity materials [12], nanotemplates [13] and catalysts [14].

In recent years, conductive polymers, including polythiophene (PT), polypyrrole (PPy) and polyaniline (PANi), have been attaching greater importance to this research. Especially PANi is easy preparation, light weight, low cost, high conductivity and chemical stability, which bring an increasing number of applications in chemical sensing, actuators, fuel cells and electromagnetic interference (EMI) shielding [15-21]. However, some applications are hindered by relative low conductivity. Therefore it is necessary to blend some other conductive materials, such as metal nanoparticles, carbon black, carbon fibers, and carbon nanotubes and so on to enhance the conductivities. Carbon nanotubes (CNTs) are of great interest because of their high electrical conductivities (10^4 S/cm) and extraordinary thermal conductivity (over 200 W/mK) [22]. Nanocomposites filled with CNTs show excellent properties and expand the application fields including semiconductors, supercapacitors, and conducting composites [23], and so on.

Some researchers have reported the relative works which have electrospun the conducting composite nanofibers from a mixture of CNTs, a PANI and poly(ethylene oxide) (PEO) blend [24,25]. Chen *et al.* [26] have prepared electrically conductive aligned polyaniline/polyimide (PI) nanofibers via electrospinning and the PANi nanoparticles were uniformly distributed on the surface of PI. Sujith *et al.* [27] electrospun highly porous PANI-carbon black composite nanofiber mats with high conductivity. In addition, it is microwave absorbing materials that are capable to absorb electromagnetic signals have been widening applied in military or commercial fields [28,29]. Fillers including metal particles and CNTs used to improve the conductivity and dielectric properties have been added in electrospun nano-composite fibers, which are investigated as microwave absorption materials. For example, Chen *et al.* [30] have presented Pd/PAN and Ag/PAN nanofibers and characterized the microwae irradiation. A system of PVA/MWCNT composite fibers has been fabricated by electrospinning method in Salimbeygi's group and the composite nanofibers with 10 % MWCNT has exhibited a reflection loss of 15 dB [31]. However, there is no report on the electrospun composite nanofiber films, which contain the polyaniline PANi and multiwall carbon nanotubes in polyacrylonitrile matrix, to investigate the microwave absorption performance. It is an effective approach that provides large surface areas, light weight, high porosity, high temperature resistance and strong interfacial strength to prepare polymer matrix composites, which may be potential to be used in aerospace (stealth aircraft), communication, environmental protection, radar, and physical protection, etc.

In this work, the electrospun PAN nanocomposite fibers with dodecylbenzenesulfonic acid (DBSA) doped PANI were obtained under appropriate conditions. The surface morphology, mechanical properties, electrical conductivity

*Corresponding author: lengjs@hit.edu.cn

and microwave absorption of the PANI/PAN/MWCNTs nanocomposite fibers were investigated by scanning electron microscopy, Van De Pauw and nanotensile tension as well as waveguide tube method.

Experimental

Materials

Polyacrylonitrile (PAN) (M_n=1,500,000) was purchased from Sigma Aldrich company. Polyaniline (PANI) (M_n= 100,000) was purchased from Sigma Aldrich. Dodecylbenzenesulfonic acid (DBSA) was selected as the doping acid. Multi-walled carbon nanotubes (MWCNTs) were purchased from Chengdu Organic Chemicals Co. Ltd. The outer diameter of CNTs was about 10-30 nm and the length was 10-30 μm. The specific surface area of the CNTs was more than 140 m^2/g. The content of -OH was about 2.48 wt%. Dimethylformamide (DMF) was used as the solvent. All the chemicals were of analytical purity and used as received without any further treatment.

Preparation of Electrospinning Solution

The electrospinning solutions of the PANI/PAN/MWCNTs with different components were prepared by dispersing the PANI, PAN and MWCNTs into DMF solvent. The ratio between DBSA and PANI was 1:3; the 3.0, 5.0 and 7.0 wt% MWCNTs solutions with PANI 0.2 wt% and PAN loadings of 8.0 wt% were obtained by magnetic stirring at room temperature for 24 h to completely dissolve the polymer.

Fabrication of PANI/PAN/MWCNTs Nanofibers

The PANI/PAN/MWCNTs nanocomposite fibers were fabricated by electrospinning. In this paper, the electrospinning apparatus was Nanospider, which could simultaneously provoke innumerable polymeric jets from a sufficiently large liquid surface to increase the productivity, as shown in Figure 1(a). The size of large area nanofiber membrane was about 600×400 mm^2. Figure 1(b) was the PAN membrane blended with PANI which was doped by DBSA and Figure 1(c) was the PANI/PAN/MWCNTs nanocomposite fiber membrane. The viscous polymer solutions were loaded in the groove, which was used for storing the electrospinning solution. The groove and electrode bar are shown in Figure 1(d). The feed rate was 0.9 mm/min and the distance was 18 cm. The high-voltage of the power was 30 to 50 kV. The electrospun nanofiber membranes were dried in an oven at 50 °C for 2 h and 70 °C for 2 h to remove any residual solvents.

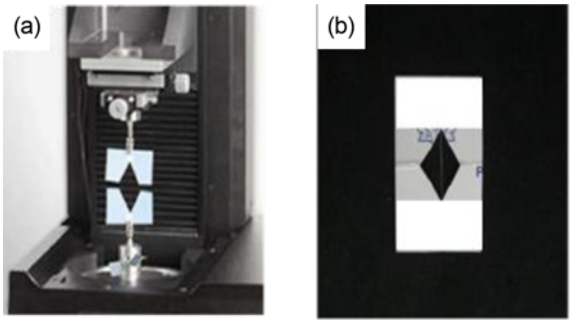

Figure 2. (a) Nanotensile testing and (b) image of the sample fixture.

Characterization

The surface morphologies of the PANI/PAN/MWCNTs nanocomposite fibers were investigated by a field emission scanning electron microscopy (SEM, Quanta 200FEG). The samples for SEM were prepared with high vacuum gold jetting for 10 min to make the surface conductive. The UV-Vis absorption spectrum was tested with a UV-Vis spectrophotometer (JENA SPECORD S600). The wavelength was from 280 to 800 nm^{-1}. The mechanical property was performed on a Nanotensile testing (Nano UTMTM Universal Testing System T150, Agilent Technologies). The tensile strain rate was set as 1.0×10^{-3} s^{-1}, and the harmonic force and the frequency were typically 4.5 mN and 20 Hz, respectively. The samples were cut into 20 mm×3 mm. The test process and sample fixture were shown in Figure 2.

Results and Discussion

In order to obtain the conductive polymers, the PANI doped with DBSA was prepared; a weight ratio of the PANI/ DBSA was 1:3. After doping, the color of solution changed

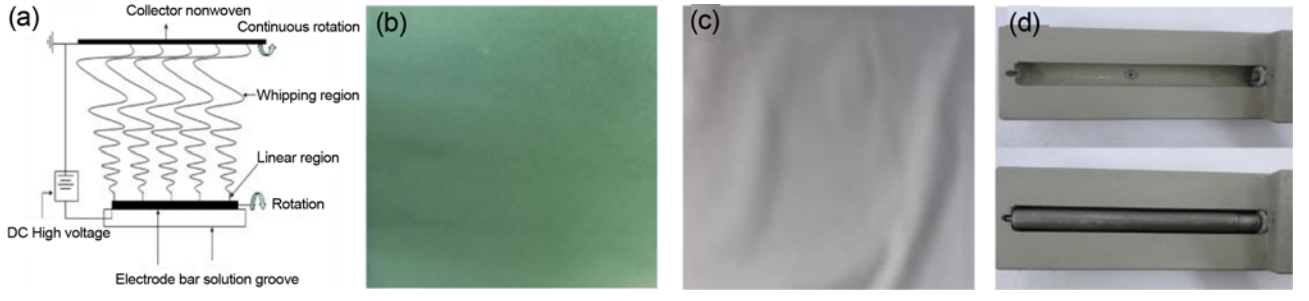

Figure 1. (a) Schematic diagram of the electrospinning setup, (b) photo of the electrospun PANI/PAN film doped with DBSA, (c) photo of the electrospun PANI/PAN/MWCNTs film, and (d) photo of groove.

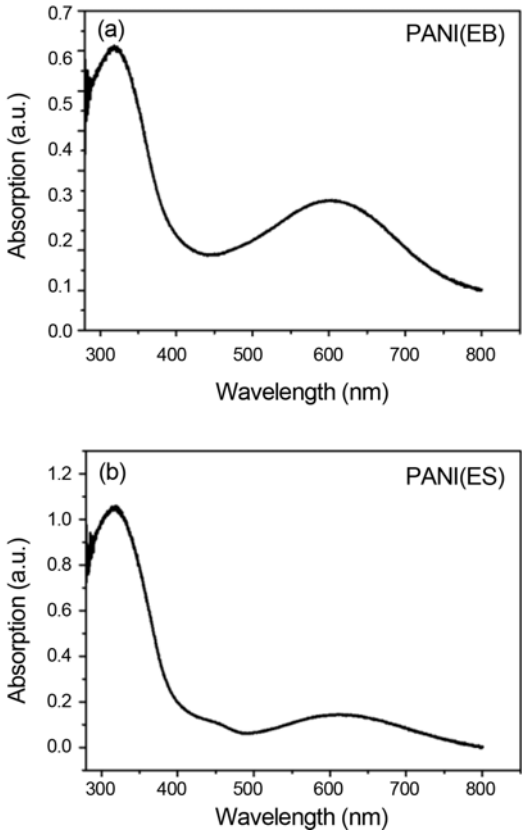

Figure 3. UV-vis absorption spectrum of the PANI/DMF solutions; (a) PANI (EB) and (b) PANI (ES).

from blue to dark green. Figure 3(a) shows the UV-Vis absorption spectra of the PANI(EB)/DMF solution. The characteristic absorption peak at 321 nm was attributed to $\pi \rightarrow \pi^*$ electronic transitions of benzene, which belonged to the B belt of phenyl structure [32]. At 606 nm, the UV absorption peak was caused by the $n \rightarrow \pi^*$ transitions, which corresponded to an indirect transition from the unit of benzene to dopaquinone [33]. As shown in Figure 3b, the absorption of the PANI (Es)/DMF solution appears. Proton acids doping triggered the absorption peak shifting from 440 to 490 nm, which generated the conjugation effect. This change affected the conductive structures of PANI. When proton acids were doped, the H^+ unites with an N atom in the chain formed a good electron delocalization, which induced the electronic cloud easily to move.

The PANI/PAN composite fibrous membranes were fabricated via electrospinning, during the process, the solvent evaporated while the polymeric jets sprayed out from the surface of the electrode to the collector of aluminum plate. The electrospinning voltage was varied at 55, 60 and 65 kV, individually, and the others were maintained constant, i.e., 18 cm spinneret-to-collector distance, and 1.5 rpm rotation rate. The electrospun solution of 0.2 wt% PANI in DMF with 8 wt% PAN was used to produce the PANI/PAN nanocomposite fibers. By visual observation, the electrospun PANI/PAN membranes appeared to be green, as shown in Figure 1(b). Figure 4 illustrates the SEM microstructures of the PANI/PAN nanocomposite fibers with increasing the applied voltage. Figure 4(a), (b) and (c) show the morphology

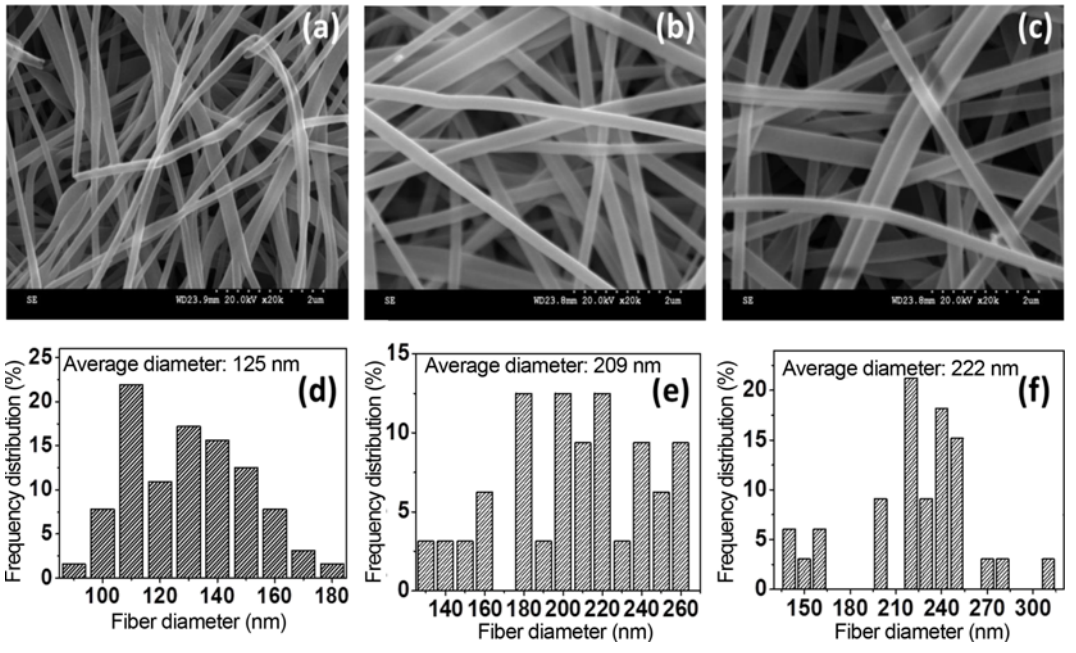

Figure 4. (a)-(c) SEM images of the electrospun PANI/PAN nanofiber membranes at a voltage of (a) 55, (b) 60, and (c) 65 kV. (d)-(f) Histograms of the electrospun nanofiber diameter distribution. Their diameters were measured using the Images J. The feed rate was 0.9 mm/min and the distance was 18 cm.

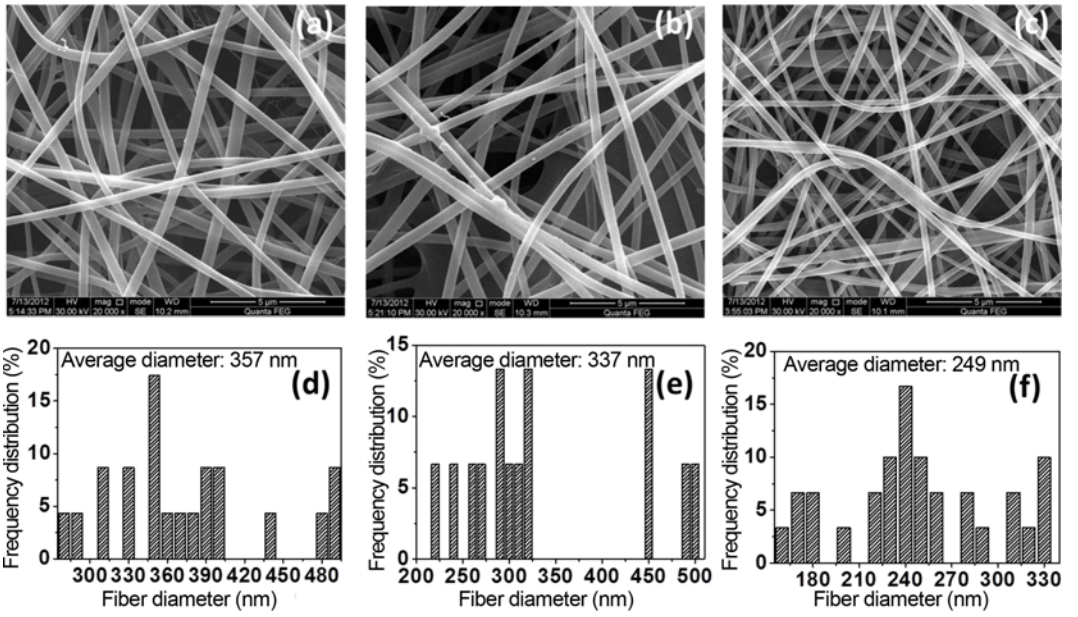

Figure 5. (a)-(c) SEM images of the electrospun PANI/PAN/MWCNTs nanofiber membrane with different MWCNTs contents: (a) 3 wt%, (b) 5 wt% and (c) 7 wt%. (d)-(f) Histograms of electrospun nanofiber diameter distribution. Their diameters measured using the Images J.

of the nanofibers at a voltage of 55, 60 and 65 kV, respectively, the results of which proved that the high quality fibers were obtained. The electrospun nanofiber membranes were highly porous in structure and ultrafine. With the voltage increasing, the fiber diameter increased from 125 nm to 222 nm. The applied voltage had a significant effect on the morphology of the nanofibers. Because more charges on the solution surface could be induced by a higher voltage, which made the solution jet fully stretched. It was consistent with the prior reports by other researches [34-37].

Figure 5 shows the surface morphology and structure of the PANI/PAN/MWCNTs nanocomposite fibers, and all samples are in fibrous structure. The incorporation of MWCNTs reduced the diameter of the PANI/PAN/MWCNTs nanofibers under the same applied voltages. The reason for this was that the addition of the MWCNTs in the polymer solution enhanced the conductivity [38]. Meanwhile, the diameter distribution range was broader. Adding 3 wt% MWCNTs, the nanofiber membrane took on black. When increasing the MWCNTs concentration to 7 wt%, the color gradually became dark, as shown in Figure 1(c). The conductive network, by increasing the MWCNTs content, was formed which induced the neighboring MWCNTs contacting. The surface morphology of the PANI/PAN/MWCNTs composite nanofibers was changed from smooth to rough gradually with the MWCNTs concentrations increasing. Perhaps some MWCNTs were not completely embedded in the PANI/PAN matrix and some protruded MWCNTs made the fiber surface rougher [38]. During the electrospinning, the MWCNTs were oriented along the elongation of the polymeric jets [39]. The distribution of the MWCNTs in the electrospinning solutions played a critical role in making MWCNTs oriented along the axes of the PANI/PAN/MWCNTs composite nanofibers.

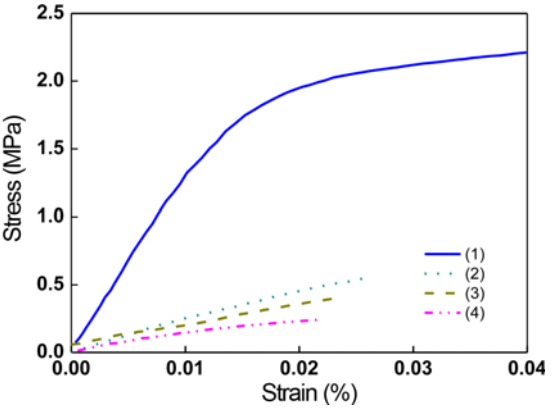

Figure 6. Engineering stress-strain responses of the electrospun films; (1) 0.2 wt% PANI/8 wt% PAN; (2) 0.2 wt% PANI/8 wt% PAN/3 wt% MWCNTs; (3) 0.2 wt% PANI/8 wt% PAN/5 wt% MWCNTs; and (4) 0.2 wt% PANI/8 wt% PAN/7 wt% MWCNTs.

To examine the static mechanical behaviors of the electrospun composite nanofiber membranes, the nanotensile testing was conducted at room temperature. The engineering stress-strain curves of the PANI/PAN and PANI/PAN/MWCNTs nanofiber membranes are plotted in Figure 6, which are quite monotonic in nature exhibiting a falling rate curve until failure. The modulus of four samples including (1) 0.2 wt% PANI/8 wt% PAN, (2) 0.2 wt% PANI/8 wt% PAN/3 wt% MWCNTs, (3) 0.2 wt% PANI/8 wt% PAN/5 wt% MWCNTs, and (4) 0.2 wt% PANI/8 wt% PAN/7 wt% MWCNTs were

Table 1. BET test results of electrospun nanofiber membranes

Sample	BET surface area (m^2/g)	Pore volume (cm^3/g)	Adsorption average pore width (4V/A by BET) (Å)
PANI/PAN film with 0 wt% CNTs	3.66	0.00094	8.56
PANI/PAN film with 3.0 wt% CNTs	4.40	0.0025	15.90
PANI/PAN film with 5.0 wt% CNTs	6.22	0.0058	35.95
PANI/PAN film with 7.0 wt% CNTs	7.10	0.0087	63.59

calculated to be 0.137, 0.04, 0.036 and 0.030 GPa, respectively. The tensile strength was 2.21, 0.55, 0.34 and 0.25 MPa, respectively. Compared with the electrospun PANI/PAN nanofiber membranes, the mechanical property of the PANI/PAN/MWCNTs nanofiber membranes decreased. While adding more MWCNTs caused the electrospun PANI/PAN/MWCNTs nanofiber membranes weaker. The difference in their mechanical property could be explained by their intrinsic morphologies. The surface areas and pore parameters of electrospun nanofiber membranes are tested via BET analysis, the results of which are shown in Table 1. From the table we can see that surface area, pore width and pore volume of membranes increase with the MWCNTs contents increasing. The low density of the nanofiber membranes with lots of pores could affect the mechanical performance. In addition, the random distribution of the MWCNTs, weak interaction between the nanofibers and the small diameter of PANI/PAN/MWCNTs composite nanofibers also caused the mechanical property decrease [40].

Under the condition of normal temperature, static resistivities of the electrospun samples were measured through a reported Van De Pauw method [41,42]. The electrical conductivity values of the samples are shown in Table 2. With increasing the MWCNTs concentration, the electrical conductivity of the PANI/PAN/MWCNTs composite nanofibers was increased. By combining MWCNTs with PANI, it is an effective strategy to improve the conductivity property for potential broadened applications.

Table 2. The resistivity of the electrospun films with different MWCNTs

Sample	Thickness (μm)	Electrical conductivity ($S \cdot m^{-1}$)
PANI/PAN film with 0 wt% CNTs	10	5.69×10^{-4}
PANI/PAN film with 3.0 wt% CNTs	30	1.79
PANI/PAN film with 5.0 wt% CNTs	25	3.26
PANI/PAN film with 7.0 wt% CNTs	20	7.97

Equations (1) to (7) were used to calculate ρ for the samples [41].

$$\rho_A = \frac{\pi}{\ln 2} f_A t_S \frac{(V_2 + V_4 - V_1 - V_3)}{4I} \quad (1)$$

$$\rho_B = \frac{\pi}{\ln 2} f_B t_S \frac{(V_6 + V_8 - V_5 - V_7)}{4I} \quad (2)$$

where ρ_A and ρ_B were the resists (Ω), t_s was the thickness, V_1–V_8 was the voltage, I was the current, and. f_A and f_B were the geometric factors, which were determined by the symmetry, and were related to Q_A and Q_B (when the samples were symmetrical, f_A=f_B=1).

Q_A and Q_B could be obtained by measuring the voltage.

$$Q_A = \frac{V_2 - V_1}{V_4 - V_3} \quad (3)$$

$$Q_B = \frac{V_6 - V_5}{V_8 - V_7} \quad (4)$$

In this paper, R_1 and R_2 were measured for 20 times, respectively.

$$R_1 = \frac{V_2 + V_4 - V_1 - V_3}{4I} = \frac{\sum_{i=1}^{20} R_{Ai}}{20} \quad (5)$$

$$R_2 = \frac{V_6 + V_8 - V_5 - V_7}{4I} = \frac{\sum_{i=1}^{20} R_{Bi}}{20} \quad (6)$$

$$\rho = \frac{\rho_A + \rho_B}{2} \quad (7)$$

Through the above analysis, the electrospun PANI/PAN/MWCNTs composite nanofibers were investigated. However, due to the low solubility of PANI and porous structures, the electrical conductivity of the composite nanofibers without MWCNTs was lower. By adding MWCNTs, it is possible to meet the need in new applications such as thermal control and infrared or radar military camouflage applications for spacecraft, electric conductive fabric, and conducting coatings.

Equations (8) was applied to evaluate reflection loss [43].

$$R_L = 20 \lg S_{11}^* \quad (8)$$

The microwave absorption of specimens was carried out using waveguide tube method, and the data was recorded by vector network analyzer under a microwave frequency range from 3.4 GHz to 18 GHz. The microwave absorption performance could be reflected from R_L. The negative value of R_L was larger; accordingly, the microwave absorption was greater [43,44]. R_L was relative to the thickness of specimens. Figure 7 shows the reflection loss of electrospun nanofiber films (0.2 wt% PANI/8 wt% PAN/7 wt% MWCNTs) in various thicknesses, including 1.0 mm, 1.5 mm and 2.0 mm, respectively. With the thickness increasing, the value of R_L

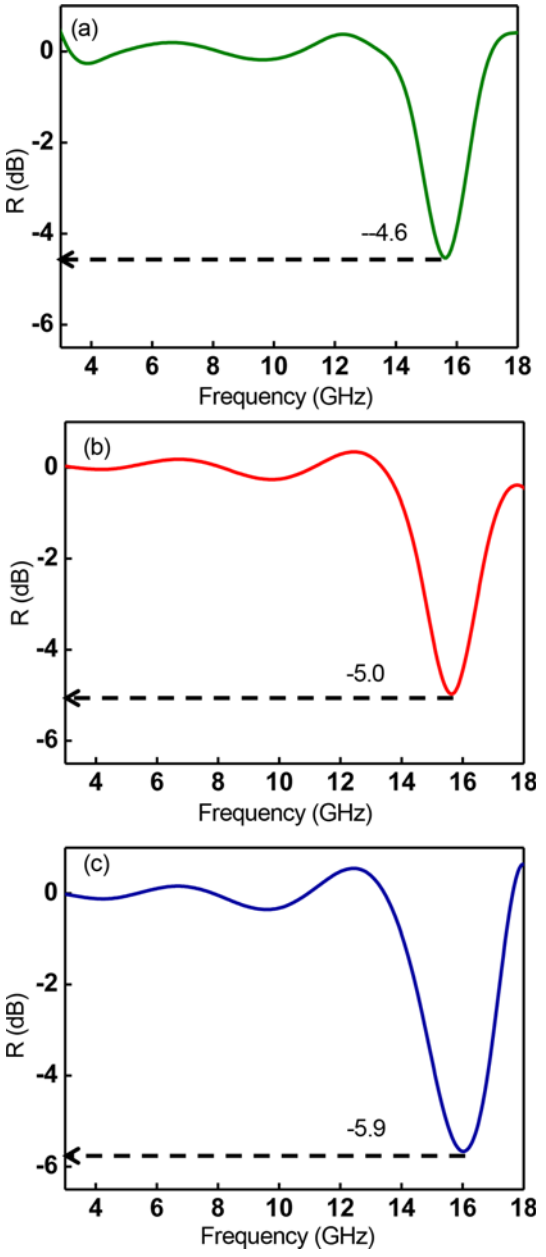

Figure 7. Microwave reflection of electrospun film (0.2 wt% PANI/8 wt% PAN/7 wt% MWCNTs) with different thicknesses.

reduced from -4.6 to -5.9 dB, which indicated that the microwave absorption intensity increased, at the same time, the absorption peak shifted to the higher frequency.

Conclusion

In this work, the PANI/PAN/MWCNTs nanocomposite fibers were successfully fabricated using electrospinning. The surface morphology of resulted samples was studied by SEM and BET, which showed the fibers were of nanoscale in diameter and uniform. The electrospun composite nanofibers demonstrated that the MWCNTs improved the electrical conductivity of the PANI/PAN nanofibers. While increasing the amount of MWCNTs, the electrical conductivity was increased. Furthermore, the PANI/PAN/MWCNTs composite nanofibers could enhance the interfacial binding force with other polymer matrixes because of the large surfaces and porous structures. These composite fibers as microwave absorption materials are promising for wide applications, such as electromagnetic shielding, radar, and protection clothes, etc.

Acknowledgements

This work is supported by the National Natural Science Foundation of China (Grant No.11225211, No.11272106, and No.51108131).

References

1. S. C. Ioannis, *J. Mater. Process Tech*., **167**, 283 (2005).
2. G. Andreas and H. W. Joachim, *Angew Chem. Int. Ed*., **46**, 5670 (2007).
3. Z. M. Huang, Y. Z. Zhang, M. Kotaki, and S. Ramakrishna, *Compos. Sci. Technol*., **63**, 2223 (2003).
4. D. Li and Y. N. Xia, *Adv. Mater*., **16**, 1151 (2004).
5. S. Yashpal, T. Ashutosh, H. Shinya, T. Dohiko, K. S. Ashok, R. Murugan, and K. Hisatoshi, *Int. J. Biol. Macromol.*, **51**, 627 (2012).
6. M. C. Chen, Y. C. Sun, and Y. H. Chen, *Acta Biomaterialia*, **9**, 5562 (2013).
7. B. Holmes, N. J. Castro, L. G. Zhang, and E. Zussman, *Tissue Eng.: Part B*, **18**, 478 (2012).
8. X. Wang, C. Drew, S. H. Lee, K. J. Senecal, J. Kumar, and L. A. Samuelson, *Nano Lett*., **2**, 1273 (2002).
9. E. R. Kenawy, L. Gary, and L. Bowlin, *J. Control Release*, **81**, 57 (2002).
10. C. Ruder, T. Sauter, T. Becker, K. Kratz, B. Hiebl, F. Jung, A. Lendlein, and D. Zohlnhofer, *Clin. Hemorheol. Micro*., **50**, 101 (2012).
11. M. Ghasemi, S. Shahgaldi, M. Iismail, Z. Yaakob, and W. R. Daud, *Chem. Eng*., **184**, 82 (2012).
12. M. Ma, Y. Mao, M. Gupta, K. K. Gleason, and G. C. Rutledge, *Macromolecules*, **38**, 9742 (2005).
13. T. Q. Liu, *J. Mater. Sci. Technol*., **20**, 613 (2004).
14. X. F. Chang, Y. Hu, and Z. L. Xu, *Mater. Lett*., **65**, 1719 (2011).
15. L. J. Zhang, M. X. Wan, and Y. Wei, *Macromol. Rapid. Comm*., **27**, 366 (2006).
16. G. M. Neelgund, V. N. Bliznyuk, A. A. Pud, K. Y. Fatyeyeva, E. Hrehorova, and M. Joyce, *Polymer*, **51**, 2000 (2010).
17. M. S. Wang, Q. Chen, and L. M. Peng, *Adv. Mater*., **20**, 724 (2008).
18. B. R. Kim, H. K. Lee, S. H. Park, and H. K. Kim, *Thin Solid Films*, **519**, 3492 (2011).

19. S. M. Ebrahim, M. M. Soliman, and M. M. El-latif, *High Perform. Polym.*, **22**, 377 (2010).
20. I. Sapurina and J. Stejskal, *Polym. Int*., **57**, 1295 (2008).
21. X. Li, S. J. Tian, Y. Ping, D. H. Kim, and W. Knoll, *Langmuir*, **21**, 9393 (2005).
22. J. Hone, M. C. Llaguno, N. M. Nemes, A. T. Johnson, J. E. Fischer, D. A. Walters, M. J. Casavant, J. Schmidt, and R. E. Smalley, *Appl. Phys. Lett*., **77**, 666 (2000).
23. Y. X. Zhou, M. Freitag, J. Hone, C. Staii, and A. T. Johnson, *Appl. Phys. Lett*., **83**, 3800 (2003).
24. M. K. Shin, Y. J. Kim, S. I. Kim, S. K. Kim, H. Lee, G. M. Spinks, and S. J. Kim, *Sensor Actuat. B*, **134**, 122 (2008).
25. B. Sundaray, A. Choi, and Y. W. Park, *Synthetic Met*., **160**, 984 (2010).
26. D. Chen, Y. E. Miao, and T. Liu, *ACS Appl. Mater. Interfaces*, **5**, 1206 (2013).
27. K. Sujith, A. M. Asha, P. Anjali, N. Sivakumar, K. R. Subramanian, S. V. Nair, and A. Balakrishnan, *Mater. Lett*., **67**, 376 (2012).
28. H. M. Kim, K. Kim, C. Y. Lee, J. Joo, S. J. Cho, and H. S. Yoon, *Appl. Phys. Lett.*, **84**, 589 (2004).
29. P. Saini, V. Choudhary, and S. K. Dhawan, *Polym. Adv. Technol*., **20**, 35 (2009).
30. J. Chen, Z. Li, D. Chao, W. Zhang, and C. Wang, *Mater. Lett*., **62**, 692 (2008).
31. S. Golestan, N. Komeil, and S. A. Mousavi, *Micro & Nano Lett.*, **8**, 455 (2013).
32. J. X. Huang, J. A. Moore, J. H. Acquaye, and R. B. Kaner, *Macromolecules*, **38**, 317 (2005).
33. A. A. Athawale, M. V. Kulkarni, and V. V. Chabukswar, *Mater. Chem. Phys.*, **73**, 106 (2002).
34. J. M. Deitzel, J. Klemmeycr, and D. T. Harris, *Polymer*, **42**, 261 (2001).
35. D. Zhang, A. B. Karki, D. Rutman, D. P. Young, A. Wang, D. Cocke, T. H. Ho, and Z. H. Guo, *Polymer*, **50**, 4189 (2009).
36. J. H. Zhu, S. Y. Wei, X. L. Chen, A. B. Karki, D. Rutman, D. P. Young, and Z. H. Guo, *J. Phys. Chem. C*, **114**, 8844 (2010).
37. X. L. Chen, S. Y. Wei, C. Gunesoglu, J. H. Zhu, C. S. Southworth, L. Sun, A. B. Karki, D. P. Young, and Z. H. Guo, *Macromol. Chem. Phys*., **211**, 1775 (2010).
38. J. R. Eun, H. A. Kay, K. K. Kim, Y. J. Seung, and H. L.Young, *Chem. Phys. Lett.*, **413**, 188 (2005).
39. Y. Dror, W. Salalha, R. L. Khalfin, Y. Cohen, A. L. Yarin, and E. Zussman, *Langmuir*, **9**, 7012 (2003).
40. H. Hou, J. J. Ge, J. Zeng, Q. Li, D. H. Reneker, A. Greiner, and S. Z. D. Cheng, *Chem. Mater*., **17**, 967 (2005).
41. V. D. Pauw, *Philips Research Reports*, **13**, l (1958).
42. J. Banaszczyk, A. Schwarz, M. G. De, and L. L. Van, *J. Appl. Polym. Sci.*, **117**, 2553 (2010).
43. S. W. Phang, R. Daik, and M. H. Abdulhah, *Thin Solid Films*, **477**, 125 (2005).
44. S. W. Phang, M. Tadokoro, J. Watanabe, and N. Kuramoto, *Synth. Met.*, **158**, 251 (2008).